Simulations and experiments of self-associating telechelic polymer solutions

2008 J. Phys.: Condens. Matter 20 335103

(http://iopscience.iop.org/0953-8984/20/33/335103)

IOP Publishing Journal of Physics: Condensed Matter

J. Phys.: Condens. Matter **20** (2008) 335103 (11pp) doi:10.1088/0953-8984/20/33/335103

Simulations and experiments of self-associating telechelic polymer solutions

M J Cass[1,3], D M Heyes[1], R-L Blanchard[2] and R J English[2]

[1] Division of Chemical Sciences, Faculty of Health and Medical Sciences, University of Surrey, Guildford GU2 7XH, UK

[2] Centre for Water Soluble Polymers, North East Wales Institute of Higher Education, Plas Coch Campus, Mold Road, Wrexham LL11 2AW, UK

E-mail: d.heyes@surrey.ac.uk and englishr@newi.ac.uk

Received 6 March 2008, in final form 5 June 2008
Published 8 July 2008
Online at stacks.iop.org/JPhysCM/20/335103

Abstract

A Brownian dynamics computer simulation study of a highly coarse-grained model of telechelic associating polymers has been carried out. In a critical concentration range the model produces the so-called 'loops-to-bridges' transition, thought to exist in the experimental systems, in which the two hydrophobic groups are in different micelles, thereby forming a highly interconnected, ultimately percolating, network. The fraction of bridged polymers produced by the model correlates well with the experimental viscosity at corresponding concentrations. The distribution of micelle sizes compares favorably with the predictions of the Meng–Russell free energy theory. The mean cluster size scales well with volume occupancy according to a simple mean-field theory. The stress relaxation function is a stretched exponential at short times and not too high concentrations but develops a longer time plateau in the percolation region, both in agreement with experiment. New experimental data for the concentration dependence of the self-diffusion coefficient, viscosity, elastic modulus and relaxation time of telechelic associative polymers are presented, which show broad qualitative agreement with the simulation data.

(Some figures in this article are in colour only in the electronic version)

1. Introduction

Water soluble polymers containing a small number of hydrophobic groups or 'stickers' are known as 'associative polymers', AP. They are known to cluster dynamically in solution forming extended supramolecular structures which give rise to significant rheology modification compared to non-associating polymers of the same backbone composition. These molecules are of immense technological importance, primarily as viscosity modifiers, in a wide range of applications, including coatings, pharmaceuticals, bio-medical fluids and personal care products (see, for example, Schultz and Glass 1991, Alexandridis and Lindman 2000). The prototype AP molecule, known as the 'telechelic' architecture, has a hydrophobic 'sticker' group at both ends of a linear polymer chain. Solutions of telechelic associative polymers show a Newtonian plateau at low shear rates, shear thickening and then shear thinning with increasing shear rate (Annable *et al* 1993, Tam *et al* 1998, Ma and Cooper 2001), which can eventually lead to instability and phase separation (Pham *et al* 1999). In dilute solution the experimental evidence is that these molecules assemble into 'flower-like' micelles in which each polymer is looped back on itself into the same micelle. With increasing concentration the micelles become increasingly interlinked by bridging polymers, a stage called the 'loops-to-bridges' transition, eventually producing a system-spanning network of bridged micelles ('percolation' transition). Stress relaxation in these systems has been envisaged to involve thermally activated disengagement of a hydrophobes from the micellar cores, followed by Rouse-like relaxation of the chains. This process can, to a good approximation, be described by a single characteristic time. Recent work on the rheology of these systems has indicated a more complex structure

[3] Present address: CDT Ltd, Building 2020, Business Park, Cambourne, Cambridge CB3 6DW, UK.

at the mesoscale, largely dependent on the level of volume occupancy of the flower micelles. Telechelic APs have been extensively studied by experiment and theory, for example, by transient network theory, TNT (Pellens *et al* 2004). While there is considerable experimental and theoretical evidence for the existence of these micelles and their various levels of association, the picture is still rather incomplete in regard to the spatial distribution of the molecules and how the assembly of micelles evolves with time, which is required to interpret in a quantitative fashion spectroscopic and rheological features. The thermodynamic underpinning of the association of the hydrophobic groups is complex, with a major contribution arising from the entropy benefit associated with the 'restructuring' of the water network on association of the hydrophobes. The topology of the network, as described by the hydrophobe aggregation number and proportion of bridged polymers of bridging chains, depends on chain length and a range of other factors associated with the chemical nature of the AP (e.g., see Hamley 2000).

Molecular modeling is able to provide further insights into the dynamical microstructure and its relationship to the physical properties. A wide variety of molecular simulation techniques has been used to model AP solutions, for example, molecular dynamics (Khalatur *et al* 1998, Velichko *et al* 1999), Monte Carlo (Groot 1994a, 1994b), and Brownian Dynamics (Xiao and Heyes 2002). A fully atomistic approach is not feasible with present computer resources and a large degree of 'coarse-graining' of the polymer is required to allow a large number of model polymer molecules to be simulated. The individual polymer molecules are commonly represented by a small number of 'beads' linked by harmonic constraining interactions along the chain. There are various models used for the interbead interactions, including the hard sphere (Groot 1994a, 1994b) and Lennard-Jones potential (Khalatur *et al* 1998, Khalatur and Mologin 2001, Guo and Luijten 2005). The polymers in these studies were highly 'coarse-grained', typically down to as few as about 10 Kuhn-length 'beads'. Nevertheless, even this small number of beads in each chain imposes severe restrictions on the scale of self-assembly of the polymer molecules and the extent of evolution in time that can be followed in a simulation. The percolation transition and the effect it has on the physical properties have not been quantitatively characterized in these previous studies. Also previous models are of rather indeterminate length and timescale.

The timestep and hence the overall timescale of the simulation is limited by the steepness of the potential, making it advantageous to use as soft an interaction as possible. This is accomplished by coarse-graining to the maximum extent possible, without losing the unique chemical signatures of the system. For non-associative polymers, effective interactions between the centers of mass of polymers have a near-Gaussian analytic form (Louis *et al* 2000a, 2000b, Addison *et al* 2005, Hansen *et al* 2005) and, because they are extremely soft, allow for a relatively large simulation timestep. As described in the next section, the current model treats the telechelic polymer chain as a pair of beads. This maximizes the number of polymers that can be simulated and lends itself to the study of processes taking place on timescales much longer than the relaxation time of a single molecule in its environment, revealing long-range structures and rheologically significant dynamical processes for the first time in simulation studies of AP molecules.

2. The model

The main task in the model construction is to develop an effective interaction between the polymer molecules in which many of the degrees of freedom at the chain level have been formally removed and whose 'average' effects are incorporated into this potential to allow for a larger window of time and length scales. This kind of coarse-graining approach has been found to be useful in understanding the important physical processes. The most rigorous route is to derive the effective potential from monomer-resolved simulations carried out on the two molecules. This has been applied to linear polymers (e.g., Louis *et al* 2000a, 2000b), diblock polymers (Addison *et al* 2005) and star polymers (e.g. see Mayer and Likos 2007, Watzlawek *et al* 1999, Lo Verso *et al* 2006 for the derivation and applications of the effective potential). The advantage of this approach is that the various configurations of the polymer chains are more properly weighted in the effective potential.

The approach adopted here is more empirical, making use of effective interactions already employed for related chemical architectures. In the most basic case, the hydrophilic block or backbone of the polymer could be treated as a single bead, able to associate to two nodes (a 'bridge') or form a double association to a single node (a 'loop'). Alternatively, the hydrophilic block could be represented by two beads, each representing a 'half-chain', and each only able to associate to a single node. The first approach, while potentially more computationally efficient, would require a rather complicated interaction law to take into account the geometric and entropic differences between looped and bridged states. In a looped state, the polymer is more compact than in an unassociated or bridged state and the excluded volume potential would thus need to have a higher amplitude for small separations, and be shorter ranged. The loss of entropy on loop formation would also require explicit inclusion in the model. The criterion governing association and dissociation of the beads to nodes would also be complicated by the requirement that one hydrophobe could dissociate while the other remained attached. The alternative approach, which is adopted here, treats the polymer as two distinct half-chains, and has certain advantages. In this approach, the change in entropy between the two states naturally emerges when the two beads are in the looped or bridged states. Also, the 'stiffness' of the polymer backbone can be adjusted by varying the intra-polymer excluded volume repulsion strength. In reality there is a degree of stretching of the chains from Gaussian statistics typically by a factor of $4/\sqrt{3}$ (Meng and Russell 2006). However, in this preliminary study, the effects of chain stretching are omitted from the model.

For the non-bonded bead interactions a single Gaussian interaction center is used, which has been shown to represent the average free energy of interaction between non-associative

polymers, at not too high concentrations (Addison *et al* 2005). The model adopted here is an extension of one proposed by the authors for asymmetric diblock copolymers (Cass *et al* 2007), hereafter referred to as 'I'. (By 'asymmetric', it is meant that the associating part of the molecule occupies a much smaller volume than the non-associating moiety.) Each telechelic molecule is represented by two beads joined by a harmonic spring. The beads interact with other beads separated by a distance, r, between their centers of mass (COM) via a repulsive Gaussian interaction,

$$U_{\rm ev}(r) = E_{\rm ev}\exp(-r^2/\sigma_{\rm ev}^2) \tag{1}$$

where $E_{\rm ev}$ and $\sigma_{\rm ev}$ are the characteristic free energy and polymer size of the interaction, respectively. The good solvent value of $\sigma_{\rm ev}/r_{\rm gyr} = 0.66$ was employed, where $r_{\rm gyr}$ is the radius of gyration of the whole chain (used as the unit length here). $k_{\rm B}T$ is the unit of energy here, where $k_{\rm B}$ is Boltzmann's constant and T is the absolute temperature. The free energy barrier height at $r = 0$, $E_{\rm ev}$, is somewhat higher here than for the case where the polymer is represented by a single Gaussian interaction, in which case, $E_{\rm ev}/k_{\rm B}T \cong 2$, (Addison *et al* 2005), and a value of 3 was used, which is in between the values for a theta solvent (2.8) and a good solvent (3.5). The structural and dynamical properties of the system were found to be relatively insensitive to the value of this energy parameter within the range, $E_{\rm ev} = 3\pm0.5$ (in units of $k_{\rm B}T$). An increase in the value of $E_{\rm ev}$ with increasing number of beads is consistent with the trend found in other multibead coarse-grained treatments of polymers using beads with a Gaussian overlap potential (Addison *et al* 2005, Xiao and Heyes 1999, 2002), in which the optimum barrier height required was found to increase with the number of beads in the chain. As the beads represent more monomer residues within the chain, the effective interactions become softer. In all the simulations carried out here, the excluded volume repulsion between the beads in the same polymer was taken to be the same as that between beads of different polymers chains. $U_{\rm ev}$ represents the reduction in the entropy of the system when the chains overlap. As it is present between beads in the same chain and is, in fact, the main driving force in the loops-to-bridges transition, which occurs when the micelles are close enough so that the hydrophobes can remain associated with other hydrophobes in the process.

The two beads in a polymer chain are held together by a harmonic potential, $U_{\rm s}$.

$$U_{\rm s} = \tfrac{1}{2}kr^2 \tag{2}$$

where r is the separation between the centers of mass of the constituent beads and k is the spring constant. Given the softness of the other potentials in the system, finite extension modifications, such as the FENE potential (Zhou and Akhavan 2004) were deemed unnecessary. For a zero natural length harmonic spring potential, the root mean square length of the spring is $l = \sqrt{\langle r^2\rangle}$, which is related to the spring constant, $k = 3k_{\rm B}T/l^2$ (Doi and Edwards 1988). This equation can be used to give an approximate value of k, when coupled with the relation $\langle r_{ij}^2\rangle = |i-j|b^2$, where i and j are the indices of the segments along the chain, r_{ij} is the separation of segments i and j, and b is the bond length between neighboring Kuhn-length segments (Doi and Edwards 1988). This treatment leads to, $k = Q/2$, where Q is the number of beads in the polymer; hence in this case for the dimer, $k = 1$, in reduced units. The viscosity can be represented in terms of a series expansion of the concentration. Simulations of the non-associative polymers with this model reproduced, within statistics, the experimentally accepted value for the coefficient of the second order term ('Huggins' coefficient, k') for a chain in a relatively good solvent ($k' = 0.35$).

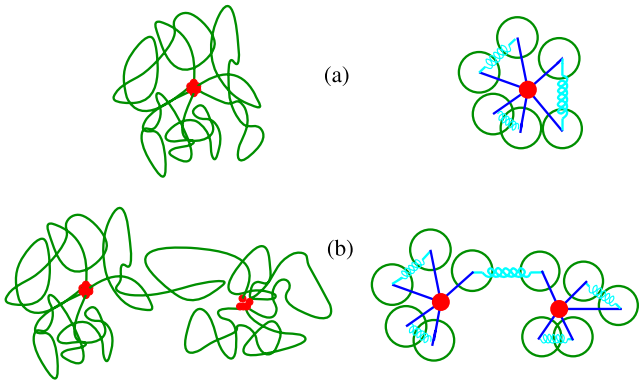

Figure 1. This figure shows the simplifications made in developing the simulation model for the telechelic polymer. Each polymer molecule is coarse-grained to the level of two beads connected by a harmonic spring potential. Each bead is capable of associating with a single node which represents the core of the micelle. There are excluded volume interactions between beads in the same and different molecules. Key: frame (a) illustrates the coarse-graining of a single 'flower' micelle, and frame (b) shows a polymer bridging between two micelles.

The micellar cores formed through association of the hydrophobes were represented in the model as a site, or node, which attracted the hydrophilic blocks through the function,

$$U_{\rm a}(x) = -E_{\rm a}\exp(-9x^2/2x_{\rm a}^2) \tag{3}$$

where x is the separation of the COM of the hydrophilic block from the node, $E_{\rm a}$ is the depth of the potential well ($E_{\rm a} = 10\pm 5\ k_{\rm B}T$ was used in the simulations), and $x_a/3$ the characteristic length scale of the interaction, which $x_a = 4$ was set. The characteristic length, x_a is approximately the distance a bead has to be from the node for it to be considered dissociated from it. The system equilibration time increases with x_a as it takes longer for the polymer to dissociate from a node. The value of $x_a = 4$ was found to be about optimum and was used in the simulations, as it was sufficiently large for micelles to form yet small enough to allow for rapid structural equilibration during a reasonable simulation timescale. $U_{\rm a}$ represents the combined effects of the attraction between hydrophobes and the resistance to stretching of the hydrophilic chain between the core of the micelle and the hydrophilic corona. The position of the nodal center of the micelle core was set to the COM of the surrounding beads. Increasing $E_{\rm a}$, lengthens the residence time of the nominal hydrophobe in the core, slowing down equilibration between loop and bridged states.

The model used to represent the telechelic polymers is illustrated in schematic form in figure 1.

There were no explicit water molecules nor any atomistic detail in the model. The free draining Brownian dynamics (BD) simulation method was used (see, e.g., Xiao and Heyes 2002) to evolve the system. The volume occupancy, $\phi = \pi r_{\rm gyr}^3 N/6V$, for N polymers in a cubic cell of volume V, was used as the measure of concentration. In trial simulations, N was varied to study the system size effects, and $N = 500$ was used in the production simulations presented here. The positions of the polymer beads were updated for ca 3–6 $\times$ 10^4 timesteps of magnitude $\Delta t = 0.1$–0.2 after an equilibration period of similar length.

The experimental data used to compare with the simulations involved a 35 kDa poly(ethylene glycol) (PEG), endcapped sequentially with a large excess of isophorone diisocyanate, followed by reaction with a linear alkanol (C_8–C_{18}) to introduce the hydrophobic moiety. Where appropriate, data for the parent unmodified PEG are included. Full details of the synthesis, purification and characterization of the polymers may be found in Hough (2003), English *et al* (2007). Depending on the endcap length (C_n), aqueous solutions of the polymers where prepared at concentrations spanning the dilute to entangled regime. Viscometric data for dilute solutions were obtained using an Ubblehode U-tube viscometer immersed in a thermostatted bath. Presenting the data in the form of the customary Huggins plot allowed calculation of the intrinsic viscosity, $[\eta]$. Treating the micelles as hard spheres allows the volume occupancy to be approximated by $\phi \sim 2/5c[\eta]$ (Pham *et al* 1999). Rheometrical data were obtained using an ARES controlled deformation rheometer or an AR-500 controlled stress rheometer fitted with appropriate concentric cylinders or cone and plate geometries. A thin film of low viscosity PDMS oil (5 cS) was applied to the edge of the sample to prevent drying out. Dynamic light scattering data (see English *et al* 2007 for experimental details) were collected using a Malvern 1000HS light scattering photometer ($\lambda = 634$ nm, $\theta = 90°$). The apparent diffusion coefficients were derived from consideration of the slower relaxation mode, assigned in this case to translational diffusion of individual flower micelles (Alami *et al* 1996, Pham *et al* 1999, English *et al* 2007). A second faster relaxation mode, usually assigned to single 'unimers', was also noted (Alami *et al* 1996).

In our comparison with the Meng and Russell theory (Meng and Russell 2005) we used the typical experimental parameters: $n_{\rm EO} = 400$ (number of ethylene oxide, EO, units per polymer half-chain), $n_{\rm c} = 12$ and 16 (number of carbon atoms per hydrophobe), $l = 0.455$ nm (hydrophobe statistical segment length); $N_{\rm c} = (n_{\rm c} + 1)/3.6$ (number of statistical segments in polymer half-chain) and $N = 3n_{\rm EO}/3.8$ (number of statistical segments in polymer half-chain).

It should be noted that in the present model, the attraction between the hydrophobes and the stretching of the polymer from the micelle core is combined into an effective attractive interaction between the polymer and the node. Therefore, while the coarse-grained model is suitable for reproducing generic trends, it does not have the atomistic resolution to define specific chemical systems, such as the number of carbon atoms in the hydrophobe, whether the hydrophobe is hydrogenated or fluorinated, or the extent of end-capping (Meng and Russell 2005). These are all important parameters in experimental systems as they determine whether two-phase separation or sol–gel (percolation) behavior (Rubinstein and Dobrynin 1999) occurs. The current model parameter set reproduces many of the general trends of the latter category. In fact, both partially and fully endcapped systems manifest the sol–gel transition for a suitable choice of hydrophobe and PEG molecular weight.

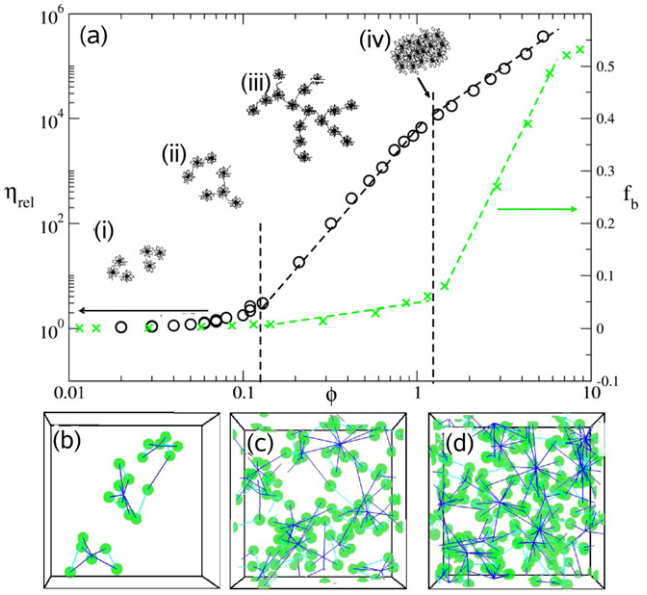

Figure 2. (a) The change of viscosity with concentration for an experimental system, shown as circles from Hough (2003), compared with the fraction of AP molecules in a bridged state, $f_{\rm b}$ (crosses and dashed curve), derived from the simulations. Also shown are schematic illustrations of the various states of self-assembly of the micelles in each concentration range. Snapshots from the simulations are shown of the self-assembly manifested at three different packing fractions: (b) $\phi = 0.08$, (c) $\phi = 0.40$, and (d) $\phi = 0.81$. The large spheres are the hydrophilic moieties, and the lines indicate their attachment to a node which represents the micelle core.

3. Results and discussion

The simulation configuration snapshots and experimental relative viscosity data are shown as a function of polymer volume occupancy in figure 2. The trends evident in the experimental viscosity, figure 2(a), and in the simulation snapshots (b)–(d) at selected ϕ values build up a mutually consistent picture of the topology and polymer dynamics of these systems. In the 'dilute regime' (figure 2(a), region (i) for ca $\phi < 0.05$), the micelles are spatially well-separated and the system has a low relative viscosity ($\eta_{\rm rel} \sim 1$). The sharp increase in the viscosity evident around $\phi \sim 0.1$ (frame (a), region (ii) for $0.05 < \phi_{\rm exp} < 0.1$) reflects the start of intermicelle bridging and the growth of clusters of micelles (cf simulation frame (b) for $\phi = 0.08$). These initial clusters are relatively long-lived, when compared to their hydrodynamic relaxation time (Rubinstein and Dobrynin

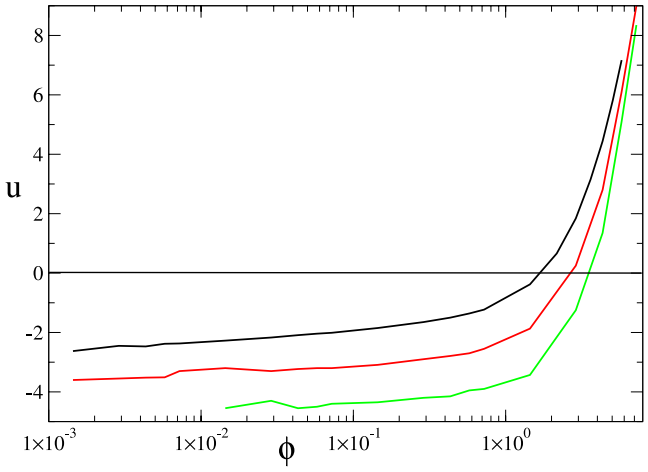

Figure 3. The average potential energy of a bead in the system, u, as a function of the packing fraction, for simulations carried out with, from top to bottom $E_a = 5$, 10 and 15.

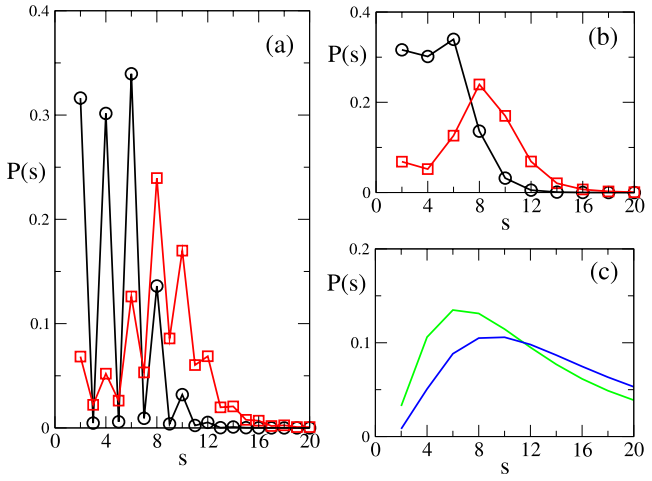

Figure 4. The probability distribution of micelle sizes, s, for two packing fractions. ○, refers to ϕ =0.014, and □ to $\phi = 0.14$. Key: (a) shows the distributions for all s, while (b) shows the distributions for micelles with only even s, (c) shows the predictions of the Meng–Russell theory (Meng and Russell 2005) for C_{12} and C_{16} hydrophobes (from left to right respectively on the figure) at unit concentration.

1999, English *et al* 2002). However, with further increase in concentration, a polydisperse ensemble of larger 'dynamic' supramicellar clusters is formed. Here, the lifetime of a typical cluster is now much shorter than its relaxation time and its structure fluctuates, constantly breaking and reforming. This regime of dynamic clusters persists through the percolation threshold, associated with the formation of a sample spanning dynamic network and an attendant sharp increase in viscosity. These data indicate that the onset of percolation is at about the same occupancy (≅0.3) in experiment and simulation (see region (iii) in frame (a), and in the stereoscopic image of frame (c)). Figure 2(c) for $\phi = 0.40$, shows a percolating cluster, involving several nodes.

Eventually the flower micelles become close-packed, which for a system of relatively small hydrophobic cores with large hydrophilic coronae takes the form of a bcc array coinciding with, the change of slope in the viscosity seen in frame (a) at $\phi \sim 1$, and in the simulation frame (d) for $\phi = 0.81$. The latter shows a more regular spacing of nodes, although close packing is not yet fully achieved at this point. In this 'close-packed' regime, the slower increase in viscosity with concentration is underpinned by an entropically-driven loops–bridges transition, as the chains become progressively more interpenetrated (Annable *et al* 1993). In addition, the coronal excluded volume repulsions become progressively more screened as the micelles become more interpenetrated.

The relationship between the viscosity data in figure 2 and the polymer microstructure discussed above is supported by the concentration dependence of the fraction of bridged chains in the system, f_b, which is superimposed on the experimental relative viscosity data in frame (a) of the figure. The transition from isolated micelles to a percolating network must be accompanied by an increase in f_b. In the dilute regime, only discrete micelles exist and hence, $f_b = 0$. In the simulations, a significant increase in f_b is seen at $\phi \sim 0.2$ (indicated by the dashed vertical line on the figure). The fraction of bridged chains in the simulation tracks the increase in viscosity throughout the 'percolation' regime until close packing at $\phi \sim 1$ (dashed line). At $\phi > 1$, the viscosity increases less rapidly with ϕ, but f_b increases more strongly, which is consistent with a loops-to-bridges transition into a close-packed array of micellar cores. Up to very high concentrations the fraction of polymers in the looped state, f_l, is negligible, with $f_l = 1 - f_b$ fitting the simulation data well. The number of 'dangling' chain ends (those that are neither bridged nor looped) in the model polymer increases dramatically for $\phi > 4$ indicating probable limitations in our simple model in this regime. An increase in the value of the parameter, E_a, promoted the looped state and delayed somewhat the rise of f_b at high packing fraction.

The close proximity of the molecules at high packing fraction is reflected in a dramatic increase in the potential energy of the system, u, and a weakening of the attraction of the node for both sticker groups, favoring bridges, as may be seen in figure 3. This figure shows that at low concentrations, u, is negative. The ϕ-dependence of u is dominated by the excluded volume contribution, which arises primarily from the packing of beads in the micelles. The contribution to u from the node-association potential is more weakly dependent on ϕ.

Distributions of the number of hydrophobes in a micelle, s, at two concentrations are shown in figure 4. Figure 4(a) presents the full probability distribution of micelle sizes, $P(s)$, while frame (b) gives $P(s)$ only for the even values of s. The dominance of loop formation at low density is evident in the distribution of micelle sizes in frame (a), as odd s value occurrences are rare. With increasing concentration, as f_b increases, the probability of odd-sized micelles increases significantly (indicative of bridging) and the position of the maximum in $P(s)$ shifts to higher values of s. The $P(s)$ distributions are similar to those seen in previous simulation studies of telechelics using multibead representations of the polymer molecules (e.g., see Guo and Luijten 2005). The predictions of $P(s)$ from the recent free energy theory of

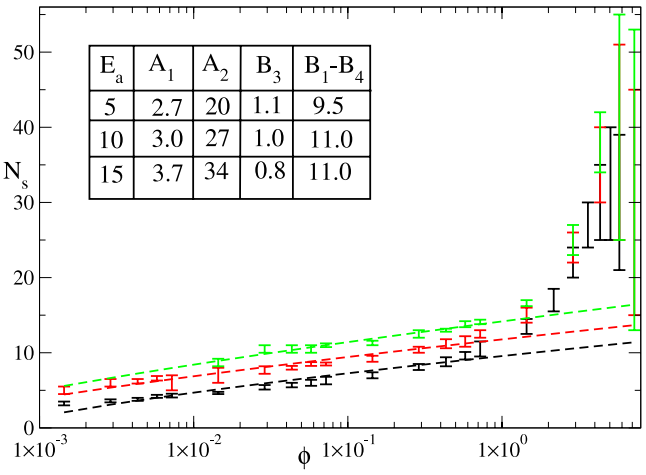

E_a	A_1	A_2	B_3	B_1-B_4
5	2.7	20	1.1	9.5
10	3.0	27	1.0	11.0
15	3.7	34	0.8	11.0

Figure 5. The aggregation number, N_s, as a function of packing fraction, ϕ, for $E_a = 15$ (upper set of data), $E_a = 10$ and 5 (lower set of data). Note that E_a sets the strength of the node–polymer interaction. The dashed lines show fits to the mean field, MF, formula given in the text and the inserted table gives the values for the fit parameters for this theory.

Meng and Russell (2005) using typical parameters for the PEG telechelics, are shown in frame (c). They are seen to agree reasonably well with the simulation data.

Figure 5 shows the average number of stickers per micelle, N_s, determined from the weight average of the number of hydrophobes attached to each node, s,

$$N_s = \sum_2^\infty s^2 P(s) \Big/ \sum_2^\infty s P(s) \tag{4}$$

N_s increases monotonically to typically about 10 at a packing fraction of unity, in agreement with dynamic fluorescence experiments (English *et al* 2007), and then increases sharply to ca 20–30 within the next decade. The value of N_s also increased with the strength of the node–polymer attraction, E_a. This figure also compares the simulation values with the prediction of a mean field, MF, formula derived in I for highly asymmetric diblock copolymers (Cass *et al* 2007, Leibler *et al* 1991). The free energy of a micelle, $\boldsymbol{F}$, is treated with the simple approximation $\boldsymbol{F} = -B_1 s + B_3 s^{4/3} - (B_3 - B_1 + B_4) + B_4 s$, where the constants represent the free energy of removing a hydrophobe from solvent (B_1), of the excluded volume repulsion between the packing of hydrophiles, (B_3), and that of loop formation (B_4). (A B_2 term representing the free energy resulting from the micelle-core surface area is neglected as the core is assumed to have negligible size.) All polymers are assumed to be looped and in micelles, which leads to the expression, $N_s^{4/3} = A_1 \ln(\phi) + A_2$, with $A_1 = 3/B_3$ and $A_2 = 3(B_1 - B_4 - 1 - B_3)/B_3$. Figure 5 shows that the MF prediction agrees well with the simulation data over many decades of concentration, even for $\phi > 0.1$ where the fraction of looped polymers steadily diminishes with increasing ϕ. The MF approximation applies well over many decades of packing fraction over which approximately all polymers are looped. A looped telechelic polymer molecule behaves in an effective sense as a single sticker polymer (i.e., asymmetric diblock) provided it does not unloop. The packing fraction needed to produce a significant fraction of bridging polymers is lower for smaller E_a and hence the point at which the MF approximation breaks down is lower for smaller E_a, as is evident on the figure.

Turning now to the dynamical behavior, the stress relaxation function, $G(t)$ is proportional to the shear stress time correlation function,

$$G(t) = \frac{V}{k_B T} \left\langle P_{\alpha\beta}(0) P_{\alpha\beta}(t) \right\rangle \tag{5}$$

where V is the volume of the system, and the notation $\langle \ldots \rangle$ indicates an average over all possible time origins. The stress tensor element, $P_{\alpha\beta}$ is given by,

$$P_{\alpha\beta} = -\frac{1}{V} \sum_{i>j} r_{\alpha ij} f_{\beta ij} \tag{6}$$

where $r_{\alpha ij}$ is the component of the vector $\mathbf{r}_{ij}$ in the α direction, and $f_{\beta ij}$ is the component of the total force between beads i and j in the β direction ($\alpha \neq \beta$ here). The summation is carried out over all pairs. Annable *et al* (1993) considered the mechanism of stress relaxation to involve a thermally activated disengagement of a hydrophobe, followed by conformational relaxation of the unentangled chains in a Rouse-like fashion, which gives an exponential ('Maxwellian') stress relaxation function, $G(t)$. This is supported by small amplitude oscillatory shear experiments with aqueous solutions of telechelic PEGs (Hough 2003). The characteristic relaxation time is sensitive to the size of the hydrophobe, through their influence on the disengagement activation energy, which should be related to the potential depth, E_a, in the present model. However, step-strain experiments have indicated a stretched exponential analytic form, $G(t) = G(0) \exp(-(t/\tau)^\alpha)$ (Cathébras *et al* 1998). Calvet *et al* (2003) carried out rheometrical experiments for telechelic fluoroalkyl PEGs and showed that the exponent, α, increased monotonically with the fraction of mechanically-active chains, which can be approximately with the fraction of mechanically-active chains, f_b. Stretched exponential behavior is also observed for other endcaps such as partially hydrogenated partially-fluorinated (Berret and Séréo 2001) and polymethyl methacrylate (PMMA) blocks (Bossard *et al* 2006).

Figure 6(a) shows the simulation $G(t)$ data and stretched exponential fits for three different volume occupancies (details are given in the figure caption). These are compared with previously published experimental curves (Calvet *et al* 2003) depicted in figure 6(b) over an equivalent concentration range. Both experimental and simulated systems exhibit stretched exponential behavior at short times, with approximately the same exponent range ($\alpha = 0.7 \pm 0.1$). At the highest polymer concentrations and long times, the simulated data show the onset of a second plateau in $G(t)$. This has also been observed in small angle oscillation for telechelic PEGs bearing alkyl and fluoroalkyl hydrophobes (Hough 2003), and has been attributed to an additional, slower mode of stress relaxation (e.g 'micelle hopping' within the close-packed array). The concentration dependence of the relaxation times,

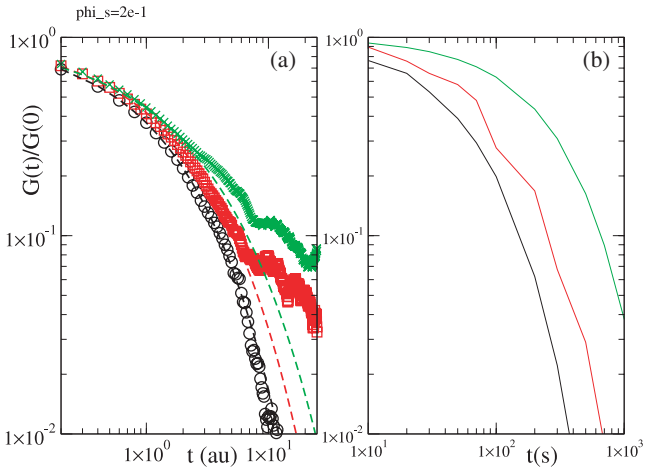

Figure 6. (a) The stress time correlation function from the simulation is shown along with stretched exponential least square fits (dashed lines), using, $G(t) = G_0 \exp(-at^{\alpha})$, with the following fit parameters: (i) O, $\phi = 0.0144$, $a = 1.02$ and $\alpha = 0.61$; (ii) □, $\phi = 0.144$, $a = 1.13$ and $\alpha = 0.70$, and (iii), ◇, $\phi = 1.44$, $a = 1.27$ and $\alpha = 0.73$. (green, red and black symbols on line). (b) Shows the experimental data of Calvet *et al* (2003) at concentrations increasing from left to right on the figure, 0.8 (black), 1.0 (red) and 1.3 (green).

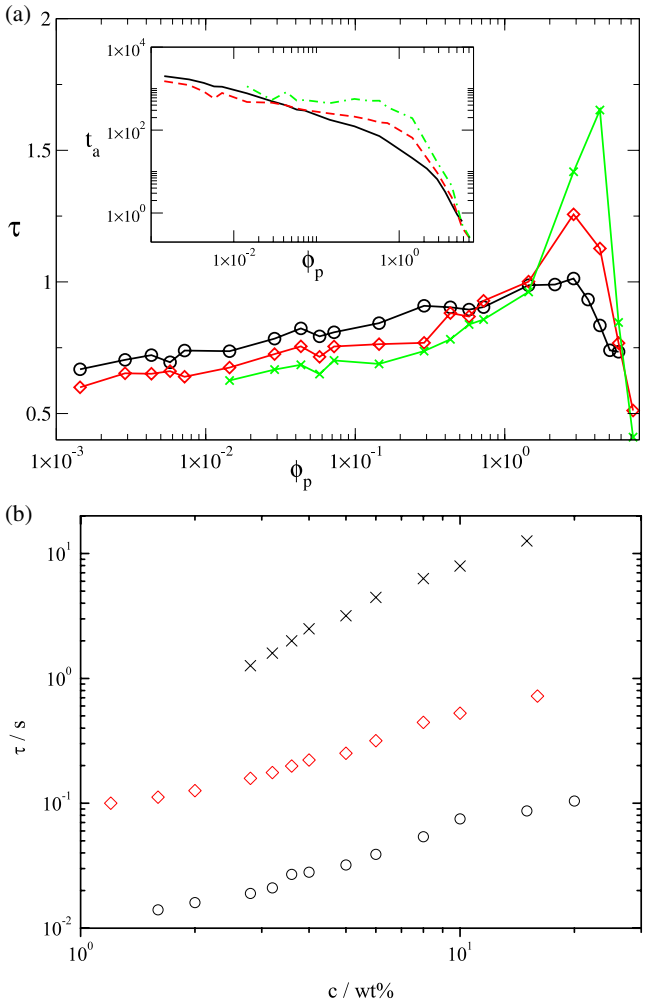

Figure 7. (a) The relaxation time of the system as a function of the packing fraction for $E_a = 5$ (O), 10 (◇), and 15 (×). The inset plot shows the average duration of association, t_a, of a bead to a node as a function of ϕ, for $E_a = 5$, solid line $E_a = 10$, dashed line and $E_a = 15$ dot–dashed line. (b) The concentration dependence of the network relaxation time derived from the rheometrical experiments of the present study on hydrophobically endcapped 35 kDa PEGs bearing larger alkyl groups—C_{16} (O), C_{18} (◇), and C_{20} (×).

τ, of the stretched exponential are shown in figure 7(a) for the simulation and 7(b) for the experiment. The relaxation time increases with ϕ as a result of the increased connection of polymers and micelles up to $\phi \sim 4$, which is probably the limit of validity of the model. Below $\phi \sim 1$ the relaxation time shows a logarithmic dependence on ϕ (i.e., $\tau \propto \ln\phi$), but above this point the time increases rapidly; how rapidly depends on the value of E_a, and in fact it follows closely the trend in f_b. The larger E_a, the steeper the rise is in τ.

The average duration of association of a polymer to a node, t_a, is shown in the insert to figure 7(a). In contrast, t_a decreases with increasing ϕ, suggesting that for higher ϕ, although individual beads are more likely to dissociate, t_a is likely to be too short to allow relaxation of the system network as a whole. The t_a were recorded directly from simulation and they show a distinct change in behavior at $\phi \sim 1$, falling rapidly above this point, which again probably indicates a limit of the validity of the model. As ϕ increases there is an increase in the number of neighboring nodes for a bead to associate with, suggesting a decrease in the likelihood of re-association to the same micelle core. From this we can infer that an increased rate of re-association would not necessarily explain the increasing trend in the relaxation time with concentration. The corresponding experimental data are shown in figure 7(b), which gives the concentration dependence of the network relaxation time derived from linear viscoelastic measurements. Both simulation and experimental values of τ increase weakly with concentration. In the experimental case, τ is calculated from the reciprocal of the frequency corresponding to the maximum in the loss modulus, G'' (Hough 2003, Annable *et al* 1993). A direct comparison between simulation and experimental data is difficult here, as viable experimental data could only be obtained for polymers with large hydrophobes (C_{16}–C_{20}) at high micellar volume fractions ($c > 1$ wt%). The network dynamics of polymers with smaller hydrophobes is too fast to be studied rheometrically by small angle oscillatory shear. Completely endcapped telechelic PEGs (35 kDa) with hydrophobes larger than C_{14} also tend to phase separate at concentrations below micellar close packing, owing to the strongly attractive intermicellar potential arising from bridging interactions (Pham *et al* 1999). Note also from figure 7(b) that the addition of two methylene groups to the hydrophobe in the experimental systems produced almost an order of magnitude increase in the network relaxation time, whereas a 5 k_BT increase in the value of E_a in simulations has a much smaller effect.

The zero shear specific Newtonian viscosity, $\eta_{sp} = (\eta - \eta_s)/\eta_s$ was calculated in the simulation using

$$\eta_{sp} = \int_0^{\infty} G(t)\,\mathrm{d}t \tag{7}$$

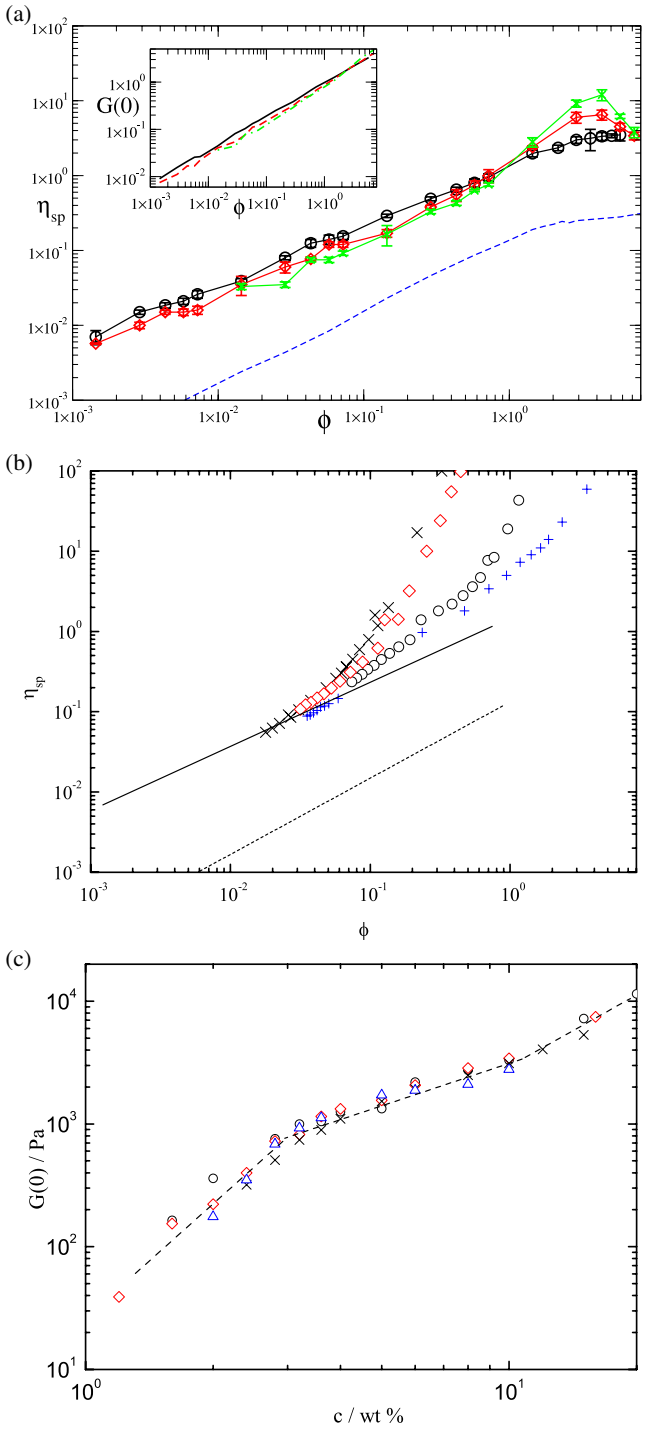

Figure 8. (a) The specific viscosity, η_{sp}, as a function of packing fraction from the simulations for, $E_a = 15$ (×), 10 (◇), 5 (O), and 0 (dashed line). The insert plot shows $G(0)$ as a function of ϕ for $E_a = 15$, dot–dashed line, 10, dashed line, and $E_a = 5$, solid line. A linear regression fit to ln η_{sp} against ln ϕ gave gradients and intercepts of (0.8, −0.28) in the case of $E_a = 5$, and (0.89, −0.27) in the case of $E_a = 10$, and (0.9, −0.52) in the case of $E_a = 15$. (b) The concentration dependence of the zero shear specific viscosity from rheometrical experiments on alkyl endcapped PEGs bearing C_8 (O), C_{10} (◇) and C_{12} (×) hydrophobes, together with the unmodified material (+). The solid line highlights the trend in the corresponding simulated data with $E_a = 5$, 10 and 15 kT to aid comparison. The dotted line shows the trend for $E_a = 0$. (c) The high frequency storage modulus, $G(0)$, measured experimentally for polymers with larger hydrophobes and therefore slower network dynamics, C_{16}–C_{20}.

in the reduced units employed solvent viscosity, $\eta_s = 1$. The concentration dependence of η_{sp} is shown as a log–log plot on figure 8(a) for three values of the node–polymer attraction parameter, E_a. It can be seen that in the concentration range below about 0.2, the viscosity increases as $\sim\phi^{0.85}$, where the exponent depends weakly on E_a. Although the model solutions are generally higher in viscosity for the larger E_a, the specific viscosity for $E_a = 10$ is lower than that for $E_a = 5$ for packing fractions below $\phi \sim 1$ but does show a steeper rise above $\phi = 0.1$. The inserted figure in figure 8(a) is a log–log plot of the infinite frequency shear modulus, $G(0)$, as a function of ϕ for different values of E_a. The exponent of ϕ for this quantity is statistically the same as for the viscosity, which suggests that the increase in viscosity is structural rather than dynamical in origin. This is because $G(0)$ is a so-called 'static' property which can be determined solely from configurational averaging and could also be computed by Monte Carlo methods (the viscosity can be written as the product of $G(0)$ and a relaxation time, which is the integral under the normalized time shear stress correlation function). Figures 8(b) and (c) provide a direct comparison between simulation and experimental data. Figure 8(b) shows the concentration dependence of the specific viscosity derived from experimental studies. A much stronger trend on sequentially increasing the hydrophobe size by two CH_2 groups (C_8–C_{12}) is seen, in comparison to the corresponding effect of increasing E_a in 5 k_BT increments in the simulations. Experiments on polymers with smaller hydrophobes facilitate comparison with simulation, as phase separation is avoided across the range of volume fractions studied ($\phi = 0.01$–5.0). Figure 8(c) shows the trend in the high frequency storage modulus, $G(0)$, measured experimentally for polymers with larger hydrophobes (slower network dynamics, C_{16}–C_{20}). These data show three distinct concentration regimes. The lowest polymer concentration regime corresponds to micellar volume fractions in excess of 0.1, falling within the percolated regime depicted in (iii) of figure 2(a). Here adding micelles to the system promotes an increase in the fraction of chains involved in intermicellar bridging and thus a more pronounced concentration dependence of the zero shear viscosity. The first inflection point corresponds to micellar overlap, with a transition to an interpenetrated regime dominated by the screening of excluded volume repulsions in the coronae ((iv) in figure 2(a)). At higher concentrations, $G(0)$ increases more rapidly again. At this level of volume occupancy, chain entanglements will start to make a significant contribution to the overall mechanical response. In addition, $G(0)$ values for all polymers derived from 35 kDa PEG bearing hydrophobes of different carbon number superpose, indicating that hydrophobe disengagement kinetics control the viscosity of the system.

The relative viscosity $\eta_r = \eta_{sp} + 1$ is plotted in figure 9(a) as a function of ϕ for different values of E_a. The increasingly steep rise in η_r with E_a at $\phi \sim 1$ as seen in the figure reflects the increasing micellar volume occupancy, and the approach of the system to close packing. The sharp downturn in the value of the viscosity for concentrations in excess of ca 1 can probably be attributed to a deficiency in the model at these high concentrations. The same monotonic increase

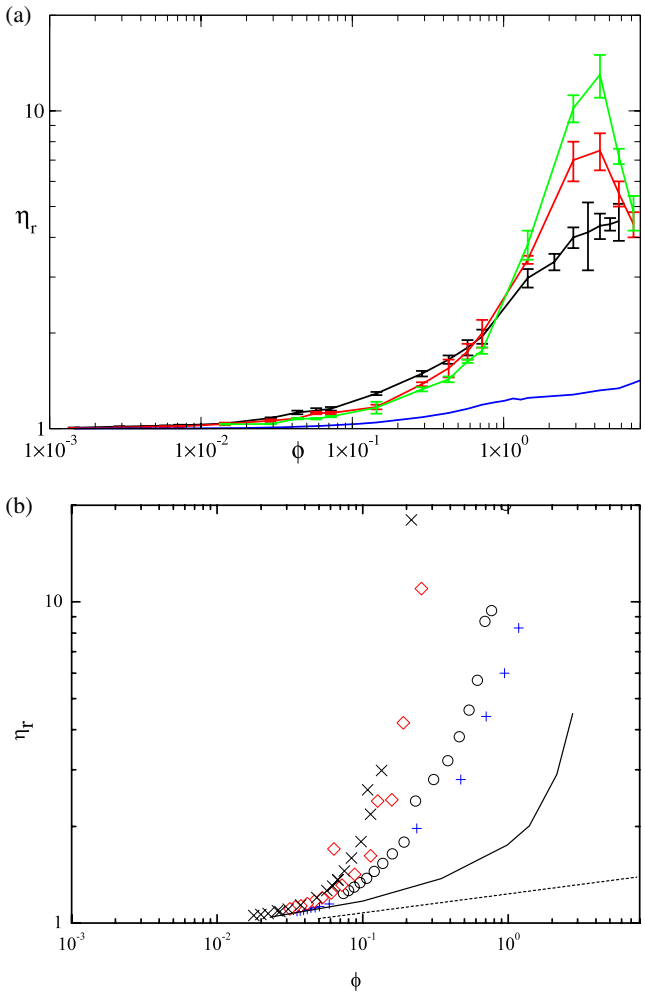

Figure 9. (a) The zero shear relative viscosity calculated from the simulation, as a function of packing fraction, for from top to bottom on the right-hand side $E_a/k_BT = 15$, 10, 5, and 0. Note the increasingly steep rise in η_r as E_a increases. (b) Concentration dependence of the zero shear relative viscosity from rheometrical experiments—parent PEG (+), C_8 hydrophobes (O), C_{10} hydrophobes (◇) and C_{12} hydrophobes (×). Solid line—corresponding trend in simulated data for $E_a/k_BT = 5$, 10 and 15. Dotted line—simulated data for $E_a = 0$.

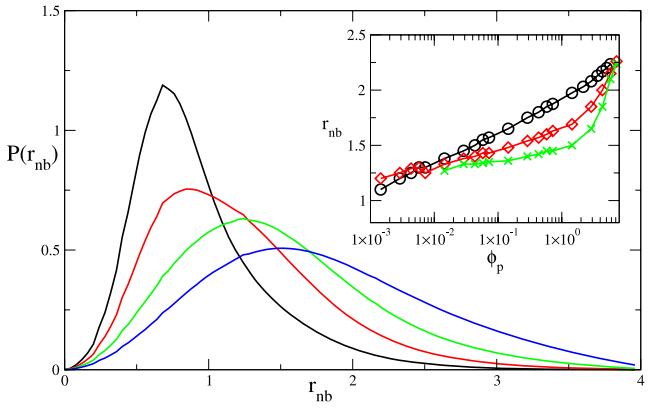

Figure 10. The average distribution of associated beads about a node at four occupancies, increasing in decades from left to right between, $\phi = 1.4 \times 10^{-4}$ and 1.4, all with $E_a = 5$. The insert shows the concentration dependence of the root mean square distance to the node of the beads. $E_a/k_BT = 5$, 10 and 15 from top to bottom.

in relative viscosity with ϕ, is present in the experimental results, as shown in figure 9(b). This figure shows data for telechelic polymers bearing smaller alkyl hydrophobes (C_8–C_{12}), together with that for the parent unmodified PEG. It is clear that the simulations underpredict the relative viscosity by around an order of magnitude. One may speculate that these differences arise because the effective intermicellar potential in the model is too soft to represent this aspect of the real system which is particularly sensitive to residue-level engagements. Also, the current model does not include the effects of the stretching of the coronal loops, for which there is considerable experimental and theoretical evidence (Alami *et al* 1996, Meng and Russell 2006), and which would make the effective interactions stiffer.

The change in N_s with ϕ is accompanied by a change in the radial distribution of beads about the node. Figure 10 shows the average probability distribution, $P(r_{nb})$, of beads about a micelle as a function of the distance from the node, r_{nb}, for four different concentrations. As the packing fraction increases, the peak of the distribution moves to larger r_{nb} because of polymer crowding in the coronal region as the micelles grow in size. The number of weakly associated beads positioned close to $r_{nb} \sim x_a$ also increases with packing fraction. Although these are formally counted as being associated to the node ('micelle'), their actual status is more questionable, as the strength of attraction to the node is probably less than the excluded volume repulsion energy experienced at this distance from the center of the micelle. The root mean square node–bead separation as a function of occupancy (given in the inset) indicates that for $\phi < 1$ the characteristic size of the micelle is approximately proportional to log (ϕ). At higher concentrations there is a steep rise for $E_a = 10$ and 15 which is possibly due to the incorporation of weakly associating beads into the micelle.

The increase in micellar size as evident in the trends in N_s and r_{nb} is reflected in a decrease in the polymer self-diffusion coefficient, D. This trend is shown in figure 11(a), for the simulation data, which also shows that D decreases with increasing E_a, reflecting the increase in the average aggregation number with E_a. The steep rise in D above $\phi \sim 3$ is probably a reflection of the finite height of the excluded volume potential. For concentrations in excess of the overlap concentration, the potential energy landscape experienced by the model polymers becomes increasingly flatter, and D in fact approaches the infinite dilution limit value. Therefore this steep rise in D at high concentrations is probably an artifact of the model which lacks residue-level detail. This trend is not seen in the comparable experimental systems, as shown in figure 11(b) for polymers bearing smaller hydrophobes (C_8–C_{12}). Here, the diffusion coefficients are normalized by the corresponding values at infinite dilution, D_0. However, the low concentration trends in D are comparable between experiment and simulation. Reference to previously published work suggests that the pronounced decrease in the

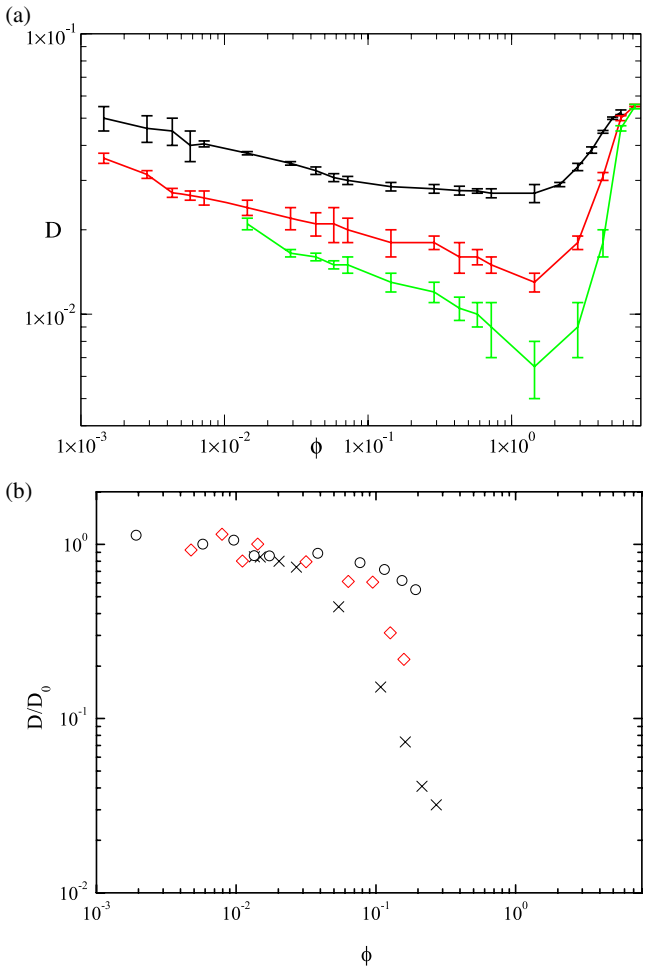

Figure 11. (a) Polymer diffusion coefficient, D, as a function of the packing fraction for association strengths of $E_a/k_BT = 5$, 10 and 15 from top to bottom. (b) Concentration dependence of the normalized diffusion coefficient, D/D_0, from dynamic light scattering experiments. Key: C_8 hydrophobes (O), C_{10} hydrophobes (◇) and C_{12} hydrophobes (×).

normalized diffusion coefficient for flower micelles formed by the C_{12} endcapped polymer is probably a consequence of the increasing viscosity of the system, rather than an increase in the hydrodynamic size. Alami *et al* (1996) showed that the hydrodynamic size of micelles formed from a C_{12} endcapped 20 kDa PEG are largely independent of concentration once changes in the macroscopic viscosity of the system were taken into account.

4. Conclusions

Despite the simplicity of the computational model it does reproduce the main trends observed for the experimental systems. For example, significant changes in self-assembled structure occur in the occupancy range between $\phi = 0.1$ and 1.0. The model predicts an increase in the fraction of 'bridged' or 'looped' chains in the system with increasing concentration, starting at a value of ca 0.1, with a percolation transition at $\phi \sim 0.3$, with close-packed micelles being present for values of ca 0.8. There is a rapid increase in the fraction of bridged polymers for concentrations in excess of 0.8, which in the experimental systems is accompanied by a more gradual increase in viscosity with concentration.

The distribution of cluster sizes is comparable to those of experimental systems and predicted by theory (see figure 4(c)). In both simulation and experiment, the viscosity increases monotonically with concentration, and the self-diffusion coefficient of the polymers decreases monotonically with increasing concentration. The stress relaxation function is of a stretched exponential form in both experiment and simulation, with statistically the same exponent (∼0.7–0.8). At high concentrations (∼1.4) both model and experimental stress relaxation functions exhibit a slower decay mechanism at long times which could be associated with slow modes arising from percolating network of micelles. The simulation elastic modulus, $G(0)$ and the shear viscosity increase by about three orders of magnitude over the studied concentration range, and as a power law of ϕ. The maximum relative viscosity in the simulation is about 10, for example. The mean relaxation time only increases by about a factor of three in the same concentration range, indicating that for the telechelic polymers the viscosity increase is mainly due to the modulus, a static property. In Maxwell's theory the viscosity is written as the product of a modulus times a characteristic relaxation time (Maxwell 1867). Even so, the increase in the viscosity from the simulation is much less than for experiment, which we attribute to the omission of almost all of the degrees of freedom of the polymer chain in the model. It is presumably mainly the interaction between the chains at the residue level that is responsible for the viscosity increase. A mean-field approximation, $\eta_{expt} = \eta_{sim}\eta_{expt,0}$, where $\eta_{expt,0}$ is the experimental viscosity of the corresponding polymer without the hydrophobic groups, still underestimates the experimental values.

There is evidence from the behavior of some of the properties (mean relaxation time, viscosity and self-diffusion coefficient) that the model is qualitatively unrealistic for occupancies in excess of ca 2–3. This is not unexpected as all mean-field 'blob' models show deficiencies in this concentration range, where the chains in the real system would be are highly interpenetrated and interactions between the chains at the residue level would dominate the physical, particularly transport, properties. The highly coarse-grained 'blob' models are too soft in this concentration region, but there is probably still scope for improvements within this basic framework.

Acknowledgments

The authors thank the Engineering and Physical Sciences Research Council of Great Britain (EPSRC) for funding this project (GR/S43771/01, GR/S43368/01). MC would like to thank Dr L Gillam and G Dear for their assistance in use of the University of Surrey's Condor PC cluster.

References

Addison C I, Hansen J P, Krackoviack V and Louis A A 2005 Coarse-graining diblock copolymer solutions: a macromolecular version of the Widom–Rowlinson model *Mol. Phys.* **103** 3045–54

Alami E, Almgren M, Brown W and Francois J 1996 Aggregation of hydrophobically end-capped poly(ethylene oxide) in aqueous solutions. Fluorescence and light-scattering studies *Macromolecules* **29** 2229–43

Alexandridis P and Lindman B 2000 *Amphiphilic Block Copolymers: Self-Assembly and Applications* (Amsterdam: Elsevier)

Annable T, Buscall R, Ettelaie R and Whittlestone D 1993 The rheology of solutions of associating polymers: comparison of experimental behavior with transient network theory *J. Rheol.* **37** 695–726

Berret J-F and Séréo Y 2001 Evidence of shear-induced fluid fracture in telechelic polymer networks *Phys. Rev. Lett.* **87** 048303

Bossard F, Aubry T, Gotzamanis G and Tsitsilianis C 2006 pH-tunable rheological properties of a telechelic cationic polyelectrolyte reversible hydrogel *Soft Matter* **2** 510–6

Calvet D, Collet A, Viguier M, Berret J-F and Séréo Y 2003 Perfluoroalkyl end-capped poly(ethylene oxide). Synthesis, characterization, and rheological behavior in aqueous solution *Macromolecules* **36** 449–57

Cass M J, Heyes D M and English R J 2007 Brownian dynamics simulations of associating diblock copolymers *Langmuir* **23** 6576–87

Cathébras N, Collet A, Viguier M and Berret J F 1998 Synthesis and linear viscoelasticity of fluorinated hydrophobically modified ethoxylated urethanes (F-HEUR) *Macromolecules* **31** 1305–11

Doi M and Edwards S F 1988 *Theory of Polymer Dynamics* (Oxford: Oxford Science Publications)

English R J, Laurer J H, Spontak R J and Khan S A 2002 Hydrophobically modified associative polymer solutions: rheology and microstructure in the presence of non-ionic surfactants *Ind. Eng. Chem. Res.* **41** 6425–35

English R J, Ratcliffe I, Blanchard R L and Parsons B J 2007 Fluorescence quenching in micelles formed by telechelic associating polymers *Macromolecules* **40** 6699–708

Groot R D and Agterof W G M 1994a Monte carlo study of associative polymer networks. I. equation of state *J. Chem. Phys.* **100** 1649–56

Groot R D and Agterof W G M 1994b Monte carlo study of associative polymer networks. II. Rheological aspects *J. Chem. Phys.* **100** 1657–64

Guo L and Luijten E 2005 Reversible gel formation of triblock copolymers studied by molecular dynamics simulation *J. Polym. Sci.* B **43** 959–69

Hamley I W 2000 *Introduction to Soft Matter* (Chichester: Wiley)

Hansen J P, Addison C I and Louis A A 2005 Polymer solutions: from hard monomers to soft polymers *J. Phys.: Condens. Matter* **17** s3185–93

Hough R L 2003 Rheology and light scattering of telechelic associating polymers derived from poly(ethylene glycol) *PhD Thesis* University of Wales

Khalatur P G, Khokhlov A R and Mologin D A 1998 Simulation of self-associating polymer systems.II. Rheological properties *J. Chem. Phys.* **109** 9614–22

Khalatur P G and Mologin D A 2001 Rheological properties of self-associating polymer systems: nonequilibrium molecular dynamics simulation *J. Mol. Liq.* **91** 205–17

Leibler L, Rubinstein M and Colby R H 1991 Dynamics of reversible networks *Macromolecules* **24** 4701–7

Louis A A, Bolhuis P G and Hansen J P 2000a Mean-field behavior of the Gaussian core model *Phys. Rev.* E **62** 7961–72

Louis A A, Bolhuis P G, Hansen J P and Meijer E J 2000b Can polymer coils be modeled as soft colloids? *Phys. Rev. Lett.* **85** 2522–5

Lo Verso F, Likos C N, Mayer C and Löwen H 2006 Collapse of telechelic star polymers to watermelon structures *Phys. Rev. Lett.* **96** 187802

Ma S X and Cooper S L 2001 Shear thickening in aqueous solutions of hydrocarbon end-capped poly(ethylene oxide) *Macromolecules* **34** 3294–301

Maxwell J C 1867 On the dynamical theory of gases *Phil. Trans. Royal Soc.* **157** 49–88

Mayer C and Likos C N A 2007 Coarse-grained description of star-linear polymer mixtures 2007 *Macromolecules* **40** 1196–206

Meng X X and Russell W B 2005 Structure and size of spherical micelles of telechelic polymers *Macromolecules* **38** 593–600

Meng X X and Russell W B 2006 Rheology of telechelic associative polymers in aqueous solutions *J. Rheol* **50** 189–205

Pellens L, Ahn K H, Lee S J and Mewis J 2004 Evaluation of a transient network model for telechelic associative polymers *J. Non-Newton. Fluid Mech.* **121** 87–100

Pham Q T, Russel W B, Thibeault J C and Lau W 1999 Micellar solutions of associative triblock copolymers: the relationship between structure and rheology *Macromolecules* **32** 5139–46

Rubinstein M and Dobrynin A V 1999 Associations leading to formation of reversible networks and gels *Curr. Opin. Colloid Interface Sci.* **4** 83–7

Schultz D N and Glass J E 1991 *Polymers As Rheology Modifiers* (Oxford: Oxford University Press)

Tam K C, Jenkins R D, Winnik M A and Khokhlov A R 1998 A structural model of hydrophobically modified urethane-ethoxylate (HEUR) associative polymers in shear flows *Macromolecules* **31** 4149–59

Velichko Y S, Vasilevskaya V V, Khalatur P G and Khokhlov A R 1999 Association of diphilic chains near the solvent critical region *J. Chem. Phys.* **111** 2340–4

Watzlawek M, Likos C N and Löwen H 1999 Phase diagram of star polymer solutions *Phys. Rev. Lett.* **82** 5289–92

Xiao C and Heyes D M 1999 The effects of bead–bead repulsion on the spatial and time correlation functions of model polymer solutions: mesoscale simulations *J. Chem. Phys.* **111** 10694–705

Xiao C and Heyes D M 2002 Brownian dynamics simulations of attractive polymers in solution *J. Chem. Phys.* **117** 2377–88

Zhou Q and Akhavan R 2004 Cost-effective multi-mode FENE bead-spring models for dilute polymer solutions *J. Non-Newton. Fluid Mech.* **116** 269–300